



PERGAMON

Journal of Quantitative Spectroscopy &
Radiative Transfer 65 (2000) 477–499

Journal of
Quantitative
Spectroscopy &
Radiative
Transfer

www.elsevier.com/locate/jqsrt

X-ray radiation from ions with K-shell vacancies

F.B. Rosmej^{a,*}, U.N. Funk^a, M. Geißel^b, D.H.H. Hoffmann^a, A. Tauschwitz^a,
A.Ya. Faenov^c, T.A. Pikuz^c, I.Yu. Skobelev^c, F. Flora^d, S. Bollanti^d, P.Di. Lazzaro^d,
T. Letardi^d, A. Grilli^e, L. Palladino^f, A. Reale^f, G. Tomassetti^f, A. Scafati^g, L. Reale^g,
T. Auguste^h, P. D'Oliveira^h, S. Hulin^h, P. Monot^h, A. Maksimchukⁱ, S.A. Pikuz^{i,1},
D. Umstadterⁱ, M. Nantelⁱ, R. Bock^j, M. Dornik^j, M. Stetter^j, S. Stöwe^j,
V. Yakushev^k, M. Kulisch^k, N. Shilkin^k

^aTechnische Universität Darmstadt, Institut für Kernphysik, Schloßgartenstr. 9, D-64289 Darmstadt, Germany

^bTechnische Universität Darmstadt, Institut für Angewandte Physik, Schloßgartenstr. 7, D-64289 Darmstadt, Germany

^cMulticharged Ions Spectra Data Center of VNIIFTRI, 141570 Mendelevo, Russia

^dENEA, Dipartimento Innovazione, Settore Fisica Applicata, 00044 Frascati, Italy

^eINFN Frascati, 00044 Frascati, Italy

^fDipartimento di Fisica e INFN g.e. LNGS, Università de L' Aquila, 67010 L'Aquila, Italy

^gInstituto Sup. Di Sanita, Roma e INFN sez Sanita, 00040 Rome, Italy

^hCommissariat à l'Energie Atomique DSM/DRECAM/SPAM, Bât. 522, C.E. Saclay, 91191 Gif-Sur-Yvette Cédex, France

ⁱCenter for Ultrafast Optical Science, Ann Arbor, Michigan, USA

^jGesellschaft für Schwerionenforschung, Planckstr. 1, D-64291 Darmstadt, Germany

^kICP Chernogolovka, Rußland, Germany

Abstract

New types of space resolved X-ray spectra produced in light matter experiments with high intensity lasers have been investigated experimentally and theoretically. This type of spectra is characterised by the disappearance of distinct resonance line emission and the appearance of very broad emission structures due to the dielectronic satellite transitions associated to the resonance lines. Atomic data calculations have shown, that rather exotic states with K-shell vacancies are involved. For quantitative spectra interpretation we developed a model for dielectronic satellite accumulation (DSA-model) in cold dense optically thick plasmas which are tested by rigorous comparison with space resolved spectra from ns-lasers. In experiments with laser intensities up to 10^{19} W/cm² focused into nitrogen gas targets, hollow ion configurations are observed by means of soft X-ray spectroscopy. It is shown that transitions in hollow ions can be used for

* Corresponding author. Tel.: + 49-6151-16-6593; fax: + 49-6151-16-4321.

E-mail address: rosmej@hrzpub.tu-darmstadt.de (F.B. Rosmej)

¹Permanent address: P.N. Lebedev Physics Institute, Russian Academy of Science, 118927 Moscow, Russia.

plasma diagnostic. The determination of the electron temperature in the long lasting recombining regime is demonstrated. In Light-matter interaction experiments with extremely high contrast (up to 10^{10}) short pulse (400 fs) lasers electron densities of $n_e \approx 3 \times 10^{23} \text{ cm}^{-3}$ at temperatures between $kT_e = 200\text{--}300 \text{ eV}$ have been determined by means of spectral simulations developed previously for ns-laser produced plasmas. Expansion velocities are determined analysing asymmetric optically thick line emission. Further, the results are checked by observing the spectral windows involving the region about the He_α -line and the region from the He_β -line to the He-like continuum. Finally, plasmas of solid density are characteristic in experiments with heavy ion beams heating massive targets. We report the first spectroscopic investigations in plasmas of this type with results on solid neon heated by Ar-ions. A spectroscopic method for the determination of the electron temperature in extreme optically thick plasmas is developed. © 2000 Elsevier Science Ltd. All rights reserved.

1. Introduction

The investigation of dense plasma has received great interest in a widespread community: inertial fusion driven by lasers and heavy ion beams, X-ray lasers, non-coherent X-ray sources, and correlation effects in dense cold plasmas. In these investigations plasma spectroscopy has provided important information for basic research and for the optimisation of desired plasma parameters. X-ray spectroscopy of these dense plasmas, which contain highly charged ions, has turned out to be extremely useful for the determination of the plasma parameters and several models have been successfully developed in the last decades, e.g. see Refs. [1,2]. The general feature of these traditional spectra are the dominant emission of resonance lines.

Recently, the interaction of radiation with matter by means of powerful lasers with extremely high contrast of up to 10^{11} produce spectra which differ dramatically from traditional ones, e.g. known from ns-laser experiments. A general feature of these newer spectra is the disappearance of the resonance lines and the appearance of very broad emission structures associated to the resonance lines. Theoretical calculations readily showed that neither Stark-broadening nor opacity effects could account for the experimental observation. Only recently, Rosmej and Faenov [3] proposed a model of accumulated dielectronic satellites (DSA-model) for the interpretation of the experimental findings [4–8].

It became immediately clear that spectra from short pulse high-power high-contrast lasers were not appropriate to study the origins of the observed spectra. Transient effects, field ionisation, continuum level depression at high densities and optical thickness made the theoretical interpretation difficult. Therefore, it was appropriate to perform experiments that could illuminate the situation and perform systematic investigations at ns-laser installation. The keypoint in these experiments being the measurement of X-ray spectra with high luminosity at high spectral and spatial resolution. This was realised by means of spherically bent mica crystals providing a spectral resolution of $\lambda/\delta\lambda \approx 10^4$ simultaneously with spatial resolution of $\delta x \approx 10 \mu\text{m}$ [9–11]. Note that spectra emitted from plasmas in traditional ns-laser experiments arising from regions close to the target surface showed emission features similar to those known from high-intensity high-contrast laser pulses.

Not all questions could be addressed in these experiments, in particular the broad emission structures located far from usual resonance line positions [12–14] required further study. A major

step the atomic data calculations that showed these structures might be due to transitions in hollow ions [7,8,14–16]. However, the question concerning the excitation mechanisms however remained unresolved.

The similarity of cold, dense plasmas created by short pulse high-contrast lasers and plasmas generated through heating solids with heavy ion beams made the beam–solid interaction experiments attractive to the laser community. Spectroscopic investigations of the first experiments with Ar-ions heating solid neon [17] were thus pursued.

2. Laser produced plasmas

2.1. Observation of unusual X-ray spectra from high-intensity high-contrast laser pulses

Experiments on the interaction of high-intensity high-contrast lasers with solid targets have been performed at the Centre for Ultrafast Optical Science of the University of Michigan [18,19]. The pulse had a duration of 400 fs, a wavelength of 0.53 μm , an energy of 1 J, and an intensity contrast of 10^{10} . The diameter of the focal spot was about 10 μm and a peak intensity of 0.5×10^{19} W/cm² was achieved at the surface of a solid target. In addition, experiments with prepulses were performed with a total energy of 2 J and a time separation from the main pulse of 2 ps. Solid Mg targets were used. X-ray spectra [19] have been recorded with spherically bent mica crystals with a 186 mm radius of curvature and X-ray CCD camera. The geometrical arrangement uses the FSSR-1D scheme [10].

Fig. 1a shows the spectral window containing the He-like resonance lines $\text{He}_\beta = 1s3p \ ^1P_1 \rightarrow 1s \ ^2S_0$, $\text{He}_\gamma = 1s4p \ ^1P_1 \rightarrow 1s^2 \ ^1S_0$, $\text{He}_\delta = 1s5p \ ^1P_1 \rightarrow 1s^2 \ ^1S_0$, and the H-like Ly $_\beta = 3p \ ^2P_{1/2,3/2} \rightarrow 1s \ ^2S_{1/2}$ lines, and the Li-like dielectronic satellites $1s3l3l'$ and $1s2l3l'$. Note that in experiments with prepulses the dielectronic satellite intensities are relatively small compared to the corresponding resonance line He_β . Similar characteristic features are seen near $\text{He}_\alpha = 1s2p \ ^1P_1 \rightarrow 1s^2 \ ^1S_0$, Fig. 1b.

With high contrast however, the situation is dramatically different. A new type of spectra develops as resonance lines disappear and the dielectronic satellites become the most pronounced emission features in the spectrum. It is obvious that spectra of this type cannot be interpreted with the traditional methods of plasma spectroscopy for a review of the traditional methods see e.g. Refs. [1,20].

These representative spectra indicate that the dielectronic satellite emission provide the key to understanding of spectra. Potentially transitions from rather exotic states, not previously considered for plasma diagnostics, may now be of great importance. This also requires that we reanalyse also traditional plasma sources, e.g. ns-laser produced plasmas, to ensure that exotic configurations are correctly and consistently included in a single computational description.

2.2. High-resolution X-ray spectra from ns-laser produced test bed plasmas: development of the dielectronic satellite accumulation model (DSA-model)

Experiments have been performed in Frascati at the HERCULES laser installation [21]. The XeCl laser had a pulse duration of 12 ns, energy 2 J, wavelength 0.308 μm and an active

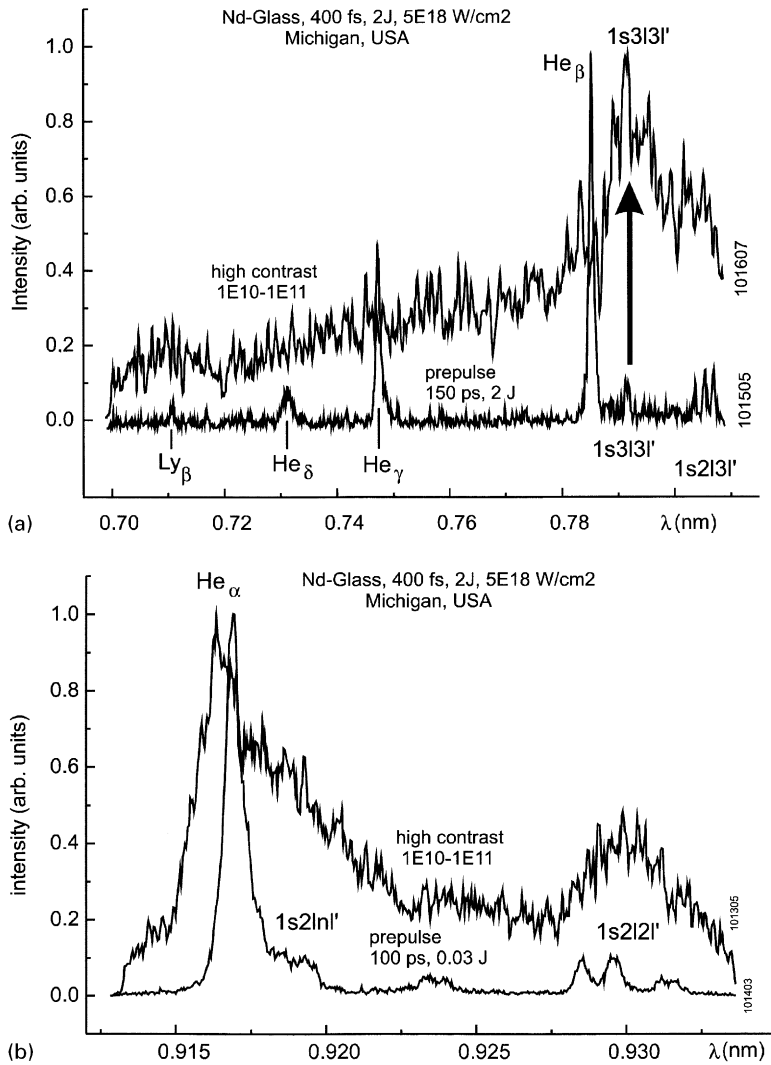


Fig. 1. (a) X-ray spectrum from high contrast laser produced plasmas and from plasmas produced with prepulses [19]. With prepulse the satellites $1s2l3l'$ and $1s3l3l'$ have weak intensity and the He-like resonance lines He_β , He_γ , He_δ and H-like Ly_β are the dominant structures in the spectrum. The spectrum with high contrast shows a dramatic difference: the dielectronic satellites $1s3l3l'$ and $1s2l3l'$ increase and dominate the spectrum whereas the resonance lines have disappeared (the digits at the right side indicate the shot number). (b) Same like Fig. 1a, however showing the X-ray spectrum [19] in the spectral window interval near the He-like resonance line He_α (recorded with a second spectrograph). With prepulse the resonance line is the dominant structure in the spectrum. The spectrum with high contrast shows a dramatic difference: the dielectronic Li-like satellites $1s2l2l'$ as well as high order satellites increase.

volume of $9 \times 4 \times 100 \text{ cm}^3$. The laser worked in a repetition mode with 10 Hz and was focused on a surface of a solid Mg target with a spot diameter of 30–70 μm , yielding a flux density of $(4\text{--}8) \times 10^{12} \text{ W/cm}^2$. X-ray spectra were recorded with spherically bent mica crystals and X-ray film. In our experiments each X-ray spectrum was the accumulation of 20–40 shots each on a fresh

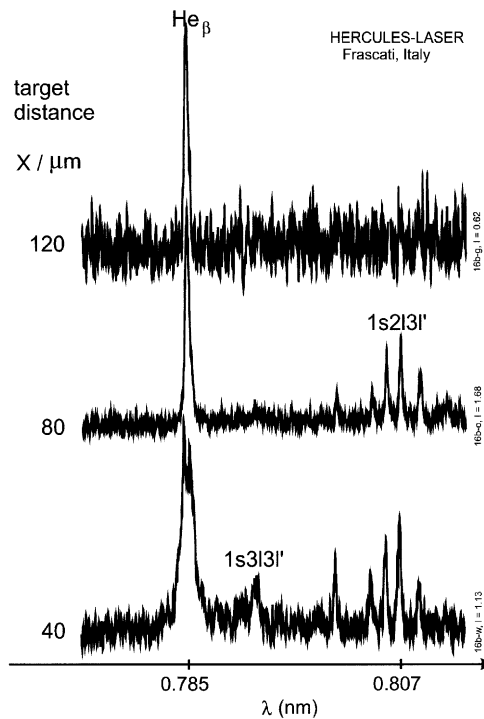


Fig. 2. X-ray spectrum from ns-laser experiment showing the spectral window near the He_β -line. Far from the target ($x > 100 \mu\text{m}$) the spectrum is dominated by the He_β -resonance line. Getting more close to the target, dielectronic satellite spectra develop strongly ($x < 40 \mu\text{m}$).

target surface. Two spherical crystals were employed simultaneously to obtain high-resolution spectra from the interval near He_α and He_β . The first spectrometer was configured according the FSSR-1D scheme [10,22] employing a crystal with curvature radius of 150 mm centred at $\lambda = 9.23\text{\AA}$. The second spectrometer geometry had the crystal, plasma and photographic film placed according the FSSR-2D scheme: crystal on the Rowland circle with both the plasma source and film placed out of the Rowland circle at a distance of 127 mm. The angle between the target surface and the spectrometer was about 20° . The curvature radius of the spherically bent mica crystal was $R = 100 \text{ mm}$. Working in the second order the Bragg angle was 52° (centred at $\lambda = 7.85\text{\AA}$). The magnification was 1 to 1. We estimated that the target position during many shots changed not more than $\pm 10 \mu\text{m}$.

In Fig. 2 space-resolved spectra arising from different distances from the target surface in the spectral range near He_β show two essential features. First, spectra far from the target (e.g. $x > 120 \mu\text{m}$) are dominated by the resonance line emission of He_β . Second, spectra close to the target (e.g. $x < 40 \text{ mm}$) show much more pronounced satellite structure, i.e. $1s3|3|'$ and $1s2|3|'$. Comparing with the spectra from Fig. 1 we infer that the intense emission of satellite spectra is correlated with plasmas close to the target surface. Thus, using these observations, together with the results from short-pulse high-contrast experiments, one can further infer that the origin of these spectra arise from the low-temperature, high-density plasmas.

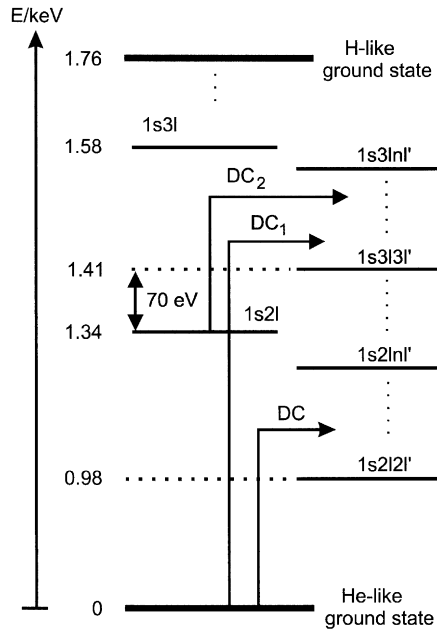


Fig. 3. Energy level diagram for the single excited He-like levels $1s2l$ and the double excited levels $1s2lnl'$ and $1s3lnl'$. $1s3l3l'$ -states autoionise not only to the He-like ground state $1s^2\ ^1S_0$ but also to the excited states $1s2l$. This results in a high electron capture to excited states due to the small energy difference of only about 70 eV.

Calculations [23,24] taking into account the dielectronic recombination to the ground state and the inner-shell excitation form the Li-like states $1s^23l$, i.e.

$$\text{dielectronic recombination: } 1s^2 + e \rightarrow 1s3l3l' \rightarrow 1s^23l' + \hbar\omega_{\text{sat}} \tag{1a}$$

$$\text{inner-shell excitation: } 1s^23l + e \rightarrow 1s3l3l' \rightarrow 1s^23l' + \hbar\omega_{\text{sat}} \tag{1b}$$

fail to describe the experimental results, the calculated satellite emission being practically absent in the simulation, in obvious contradiction to the data.

To address the lack of agreement between the calculations and the experiments we revisit the coupling of the autoionizing states in the kinetics model. Fig. 3 shows the energy level diagram for the single excited states $1s2l$ and the double excited states $1s2lnl'$ and $1s3lnl'$. The important difference between these configurations is that the configurations $1s2lnl'$ lie above threshold only to the ground state, whereas the $1s3lnl'$ -levels lie above the ground state and also above the states $1s2l$. Thus, the $1s3lnl'$ -levels can autoionize to excited states and the principle of detailed balance indicates that dielectronic capture from excited states $1s2l$ is possible. In calculated spectra simulations the relative importance of the various channels of excitation can be investigated. For this purposes we employ the MARIA-code [25]: a metastable resolved multilevel multi-ion stage collisional radiative model, having a completely transient treatment all ground stages as well as all excited states, and includes opacity effects and non-Maxwellian velocity distributions. This kinetics model allows the study of plasmas where widely disparate time scales operate in the rate equations

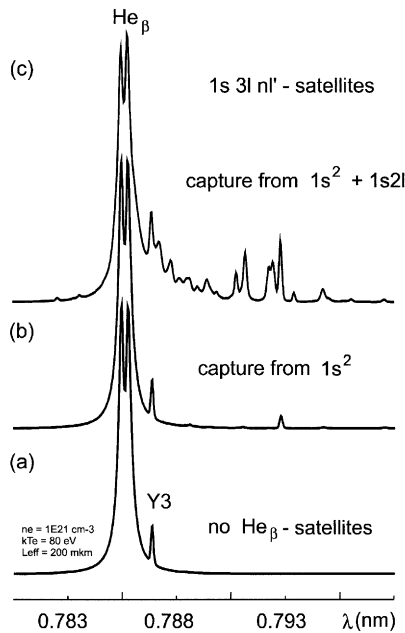


Fig. 4. Theoretical MARIA-code calculations of the He_β -line and its adjacent dielectronic satellites switching off successively various excitation channels: (a) all dielectronic satellites are switched off, (b) dielectronic capture to the He-like ground state is included, (c) also the dielectronic capture from the single excited states $1s2l$ are included resulting in a strong excitation of these satellites for plasma conditions met near the target surface, $n_e = 10^{21} \text{ cm}^{-3}$, $kT_e = 80 \text{ eV}$, $L_{\text{eff}} = 200 \text{ }\mu\text{m}$.

(see e.g. see Ref. [26] for a treatment of resonance and spin forbidden lines). The level structure is entirely dynamic, adaptable to any problem and limited only by computer memory (typical memory/disc requirements are 0.2–1 and 1–5 Gbyte, respectively). An LSJ-selective method is implemented that can exclude particular levels and excitation mechanisms even inside one LS-configuration. More details and applications are described elsewhere [6,7,16,23,27–29].

Fig. 4 shows the relative importance of the various channels for typical plasma parameters found near the target surface. In Fig. 4a all satellite transitions are excluded and the emission is dominated by the optically thick opacity broadened He_β -line. The intercombination line $Y3 = 1s3p^3P_1 - 1s^2\ ^1S_0$ is very narrow because its optical depth is very small. Fig. 4b is calculated including the dielectronic capture from the ground states (Eq. (1a)) and the inner-shell excitation (1b). The atomic structure calculations include all configurations of the type $1s3l3l'$, $1s3l4l'$, $1s3l5l'$ and $1s3l6l'$ [23]. However, it is seen that dielectronic satellites do not develop substantially. Fig. 4c shows the inclusion of the dielectronic capture to the excited states $1s2l$, and a strong increase of the satellite line formation results.

The relative importance of the dielectronic capture from excited states can be estimated followed analytically. The intensity I of a dielectronic satellite based on the dielectronic capture channel only is given by

$$I_{\text{sat}}^{\text{DC}}(a) = n_e n(a) b(a) \langle \text{DC}(a) \rangle. \tag{2}$$

n_e is the electron density, $n(a)$ is the population density of the state “ a ” into which capture is considered, b is the branching factor for the emission of a photon and $\langle DC \rangle$ is the rate coefficient for the dielectronic capture. The dielectronic capture rate coefficient is given by

$$\langle DC(a) \rangle = 1.656 \times 10^{-22} \Gamma(a) \frac{g_{\text{sat}} \exp(-E_s(a)/kT_e)}{g_a (kT_e)^{3/2}} [\text{cm}^3 \text{s}^{-1}], \tag{3}$$

where Γ is the autoionizing rate into the state “ a ” in $[\text{s}^{-1}]$, g_a and g_{sat} are the statistical weights of the capture level and the autoionizing level, respectively, E_s is the capture energy in (eV), and kT_e is the electron temperature in (eV). The intensity ratio R of the dielectronic satellite emission associated correlated to the excited states $1s2l$ and that associated to the ground state $1s^2$ is therefore given by

$$R = \frac{I_{\text{sat}}^{\text{DC}}(1s2l)}{I_{\text{sat}}^{\text{DC}}(1s^2)} = \frac{n(1s2l) g(1s2l) \Gamma(1s2l) b(1s2l) \langle DC(1s2l) \rangle}{n(1s^2) g(1s^2) \Gamma(1s^2) b(1s^2) \langle DC(1s^2) \rangle}. \tag{4}$$

The branching ratios are the same because we consider one transition but in different channels. The capture energies are related by (see Fig. 3):

$$E_s(1s^2) \approx \Delta E + E_s(1s2l), \tag{5}$$

where ΔE is the excitation energy of the $1s2l$ -levels from the ground state. The maximum population ratio can be calculated using the Boltzmann-ratio, i.e.,

$$\frac{n(1s2l)}{n(1s^2)} = \frac{g(1s2l)}{g(1s^2)} \exp(-\Delta E/kT_e). \tag{6}$$

Inserting Eqs. (3), (5) and (6) into Eq. (4) we obtain

$$R_{\text{max}} = \frac{g(1s2l) \Gamma(1s2l)}{g(1s^2) \Gamma(1s^2)}. \tag{7}$$

Table 1 shows the atomic structure calculation carried out with the Hartree–Fock method [30], where intermediate coupling, configuration interaction and relativistic corrections up to the second order have been taken into account. The autoionizing rates $\Gamma(1s2l)$ are about 2 orders of magnitude larger than the $\Gamma(1s^2)$ -rates. The maximum intensity ratio for the different channels can therefore reach factors of up to $R_{\text{max}} \approx 3 \times 10^3$. Thus, one would expect that in high-density optically thick

Table 1
Configuration averaged autoionising rates of the double excited states $1s3lnl'$ for Mg to different channels $a = 1s^2$ and $1s2l$

| Configuration | $\Gamma(1s^2)/\text{s}$ | $\Gamma(1s2s^1S_0)/\text{s}$ | $\Gamma(1s2s^3S_1)/\text{s}$ | $\Gamma(1s2p^1P_1)/\text{s}$ | $\Gamma(1s2p^3P)/\text{s}$ |
|---------------|-------------------------|------------------------------|------------------------------|------------------------------|----------------------------|
| $1s3l3l'$ | 5.6×10^{11} | 1.0×10^{13} | 3.1×10^{13} | 5.5×10^{13} | 1.7×10^{14} |
| $1s3l4l'$ | 1.2×10^{11} | 2.1×10^{12} | 6.2×10^{12} | 1.0×10^{13} | 3.0×10^{13} |
| $1s3l5l'$ | 4.1×10^{10} | 7.7×10^{11} | 2.2×10^{12} | 3.6×10^{12} | 1.0×10^{13} |
| $1s3l6l'$ | 1.8×10^{10} | 3.4×10^{11} | 9.8×10^{11} | 1.5×10^{12} | 4.5×10^{12} |

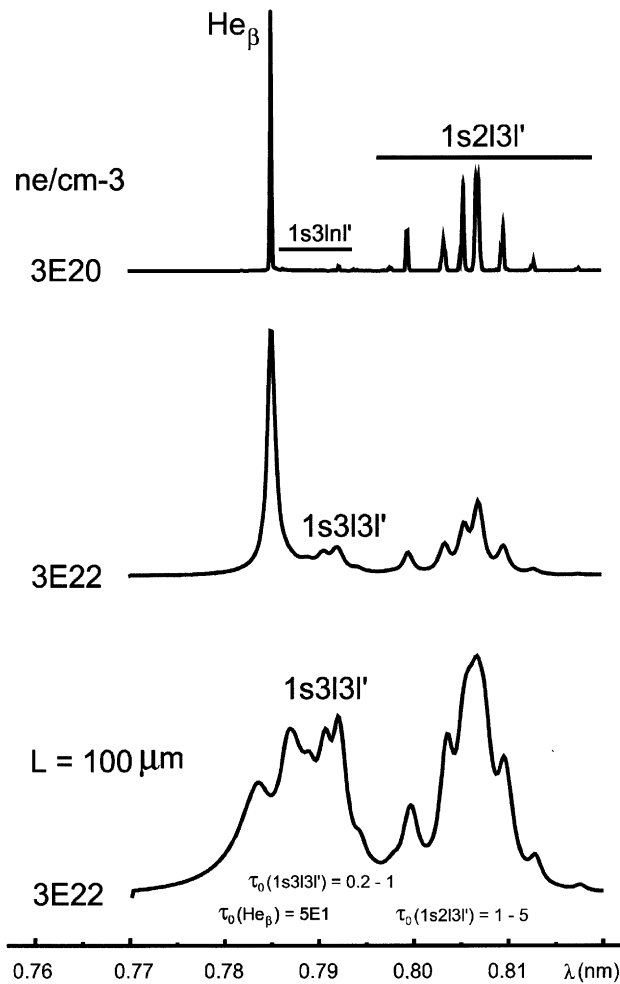


Fig. 5. MARIA-code calculations showing the development of the strong satellite emission in short pulse high contrast laser experiments. With increasing density and fixed temperature $kT_e = 100$ eV the population of the excited states $1s2l$ increases resulting in a strong dielectronic capture into the $1s3lnl'$ -states. With opacity effects included the satellite spectra dominate the emission spectrum.

plasmas R would be large because the population of the $1s2l$ increases with increasing density and due to photoabsorption of the resonance line $W = 1s2p \ ^1P_1 - 1s^2 \ ^1S_0$. Values R close to R_{max} can actually occur of a wide range of accessible densities as depicted in Fig. 5 (compare with Fig. 1a). We note that all calculations, as in Fig. 5, have been carried out using the collisional radiative model, *not* the simple form according Eqs. (2)–(7). The fact that populations of autoionizing levels are strongly correlated with single excited states of the highly charged ions has implications for other processes, not only the dielectronic capture [31,5].

Fig. 6 shows the final spectrum fitting carried out with the MARIA-code of the He_β -line and its adjacent dielectronic satellite spectra for the experimental spectrum recorded at $x = 50 \mu m$.

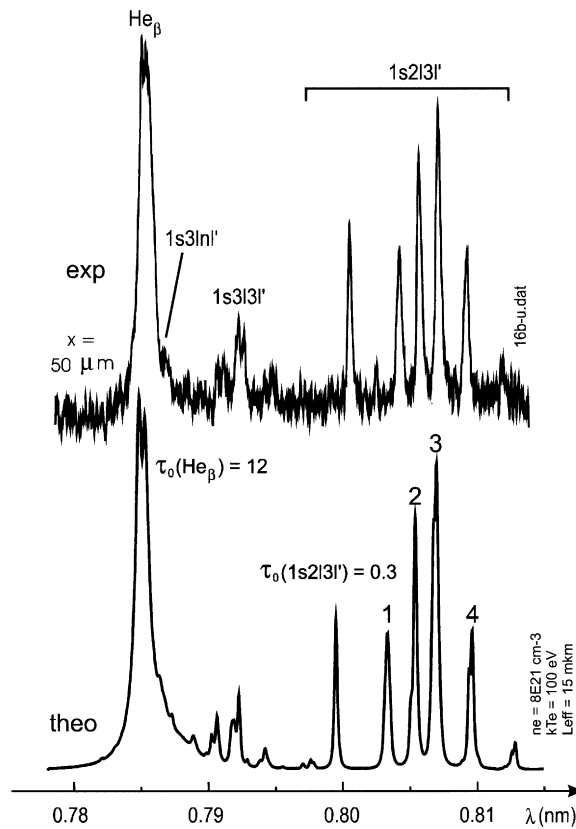


Fig. 6. Spectrum fitting of the He β -structure of ns-laser experiments carried out with the MARIA-code. Excellent agreement is seen not only for the He β -line but also for the details of the satellite emission 1s3lnl' and 1s2l3l'.

Excellent agreement is obtained for the He β -line and all dielectronic satellites of the type 1s3lnl' and 1s2l3l'. This agreement provides validation of the model we have proposed to explain the enhanced satellite emission.

Moreover, we have also cross checked our results with the He α -spectrum recorded with a second spectrometer. These spectra are shown in Figs. 7a and b. Very close to the target (e.g. $x < 50 \text{ mm}$) a complicated W-line structure develops. This structure is characterised by the disappearance of the resonance line emission and the appearance of a very broad emission structure. Fig. 7b compares, in more detail, the spectra from plasmas near to and far from the target surface. Fig. 8 shows the principle mechanism for the origin of spectra of these kind. The resonance line at position λ_0 is trapped due to high optical thickness. Excitation of double excited levels results in transitions located mainly on the red side of the resonance line caused by the screening of the nuclear charge spectator electrons. Under typical conditions found near the target surface, $n = 2$ satellites are optically thick. Even small values of optical depth, i.e., between 1 and 10, result in large reductions of the intensity due to the autoionizing probability [32]. The relative intensity of the satellite series 1s2lnl' therefore does not scale like n^{-3} as is expected from the dielectronic

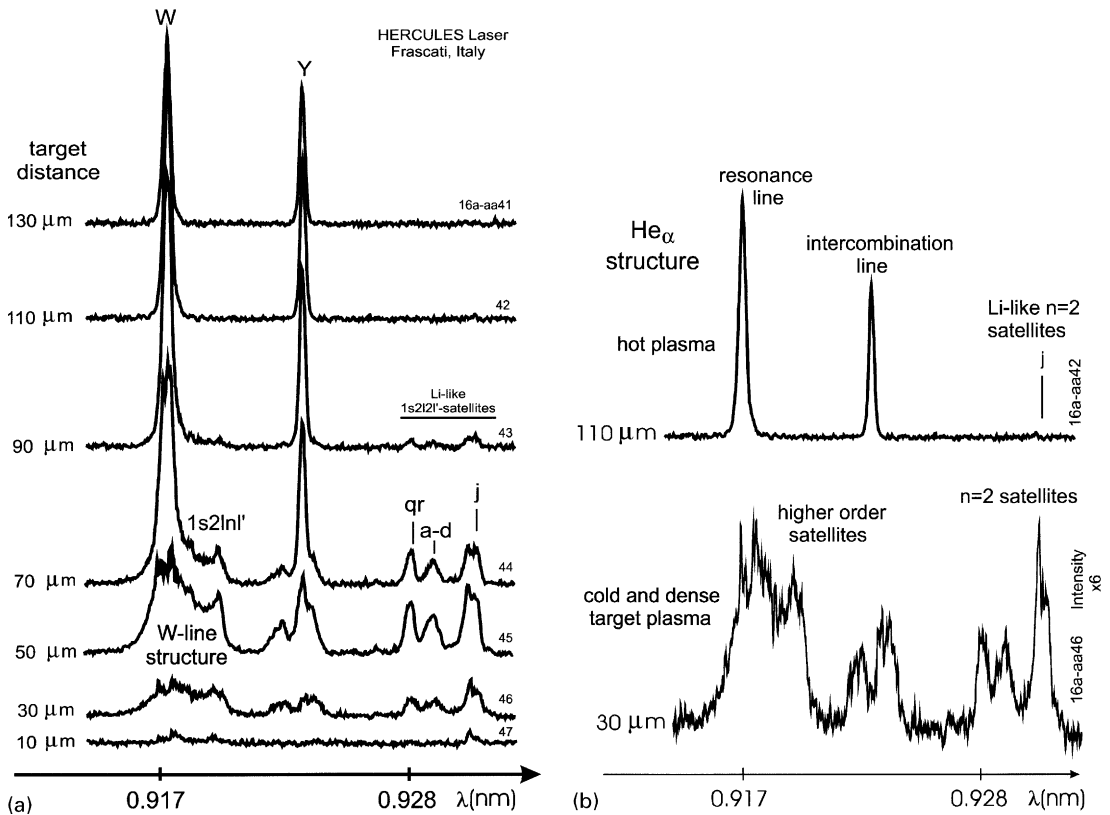


Fig. 7. Experimental spectra of the He $_{\alpha}$ -structure recorded with a second spectrograph. Close to the target, the complicated W-line structure develops.

recombination mechanism. This leads to an effective dielectronic satellite accumulation, the so-called DSA-model [3] and also to an relative enhancement of the so-called “blue satellite structure” [5,31,33]. Fig. 9 shows the development of the He-like resonance line W based on the DSA-model. It is clearly seen that this model reasonably describes the broad W-line structure. Fig. 10 shows the cross check for the He $_{\beta}$ -simulation. Taking the same simulation parameters given in Fig. 6 we obtain good agreement with the experimental results: the MARIA-code calculations are obviously bracketed by the data at $x = 30\text{--}50\ \mu\text{m}$. Deviation are certainly within the limits of the experimental uncertainties as it is difficult to adjust two spectrographs at different mean angles to look exactly into the same plasma volume.

2.3. Solid density plasma produced with high-intensity high-contrast lasers

The theoretical analysis of dielectronic satellite emission developed in Section 2.2 provides the necessary tools for the spectroscopic analysis of plasmas produced by high-intensity high-contrast laser pulses. Fig. 11a shows the spectrum from the He $_{\beta}$ -line to the Lyman continuum. There are two

dielectronic satellite accumulation

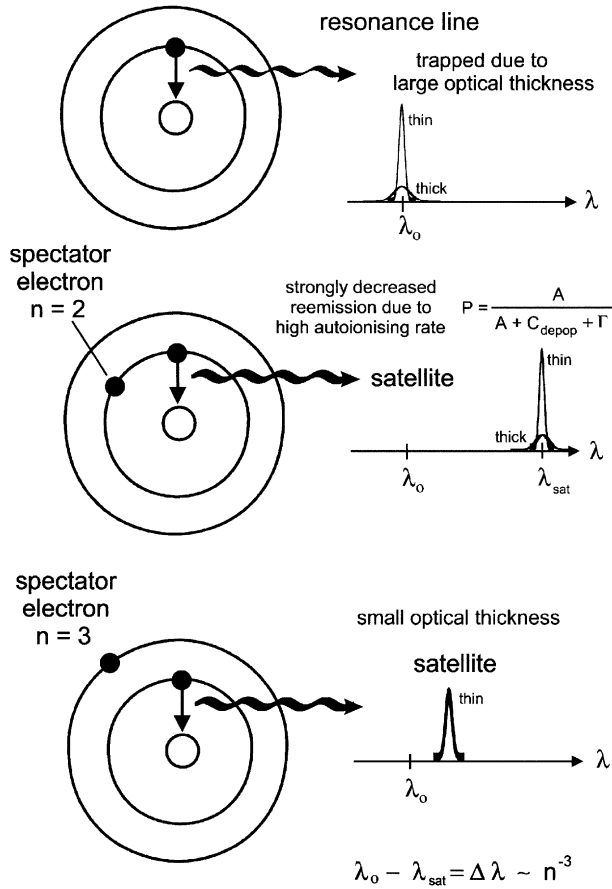


Fig. 8. Principle mechanisms for the dielectronic satellite accumulation model (DSA-model). Large optical depth in the resonance line and much smaller depth for higher-order satellites results in a strong relative increase of the satellite emission.

dominant features: 1. An intense structure near a wavelength of about 0.79 nm and a strong increasing “slope” from lower to higher wavelength.

Also shown in Fig. 11a is the calculation carried out with the MARIA-code. Good agreement for the entire spectral range is obtained for $n_e = 3 \times 10^{23} \text{ cm}^{-3}$ and $kT_e = 180 \text{ eV}$. The simulations display not only the emission close to the He_β -line but also the total slope of the emission (the experimental intensity decrease at about 0.81 nm is an artefact and caused by the end of the spectral interval). Due to high density, the continuum edge is shifted and higher He-like resonance lines have disappeared. Calculations of line merging [34] are consistent with the determined electron density we have determined. In the calculations all satellite transitions of the type $1s2i3l'$, $1s2i4l'$, $1s3i3l'$ and $1s3i4l'$ are included and are found to be essential for the fitting of the overall structure

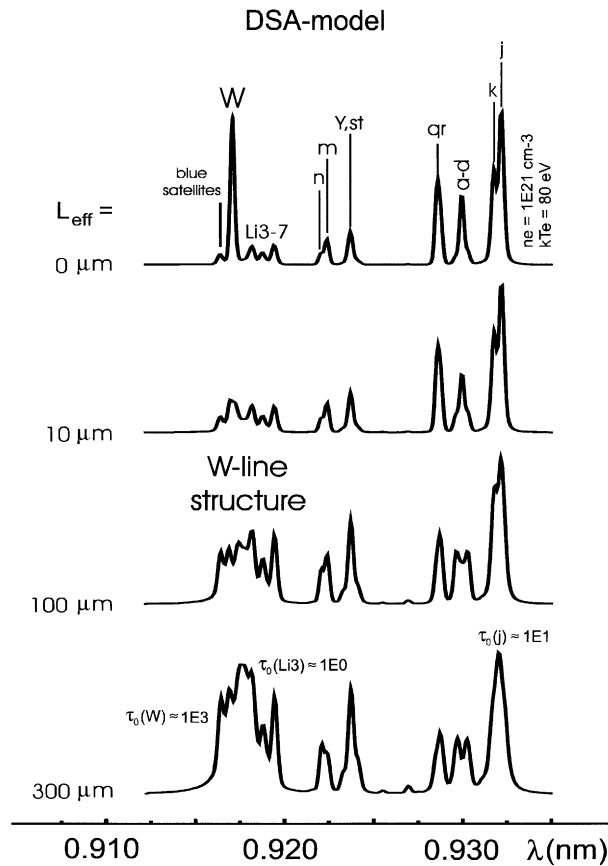


Fig. 9. MARIA-code calculations showing the satellite accumulation based on the DSA-model.

near He_β . Due to their incorporation the asymmetric wing structure near He_β could be studied: differential plasma movement in optically thick plasmas (the effective source size of $10\ \mu\text{m}$ was used, being in agreement with the laser spot size) is partly responsible, the determined expansion velocity is about $10^8\ \text{cm/s}$.

We have cross checked the theoretical results by analysing the spectral distribution near He_α . Fig. 11b show the experimental spectrum. A remarkable feature being the strong decrease of the blue wing of the He_α -structure and the falling slope on the red side. This is a result of differential motion in optically thick plasmas: Photons emitted in the plasma centre at the blue wing experience only little photoabsorption because the absorbing ions move outwards. The absorption coefficient therefore shift to the red and blue photons can more easily escape from the plasma thus causing the step rise of the blue wing. The red photons are effected in the opposite manner. Fitting the observation with the calculations gave the following parameters: $n_e = 4 \times 10^{23}\ \text{cm}^{-3}$, $kT_e = 300\ \text{eV}$, $V = 3 \times 10^7\ \text{cm/s}$ (the effective source size being $3\ \mu\text{m}$). Taking into account $A(\text{He}_\alpha) = 1.95 \times 10^{13}\ \text{s}^{-1}$ and $A(\text{He}_\beta) = 5.49 \times 10^{12}\ \text{s}^{-1}$ and the larger line broadening of the

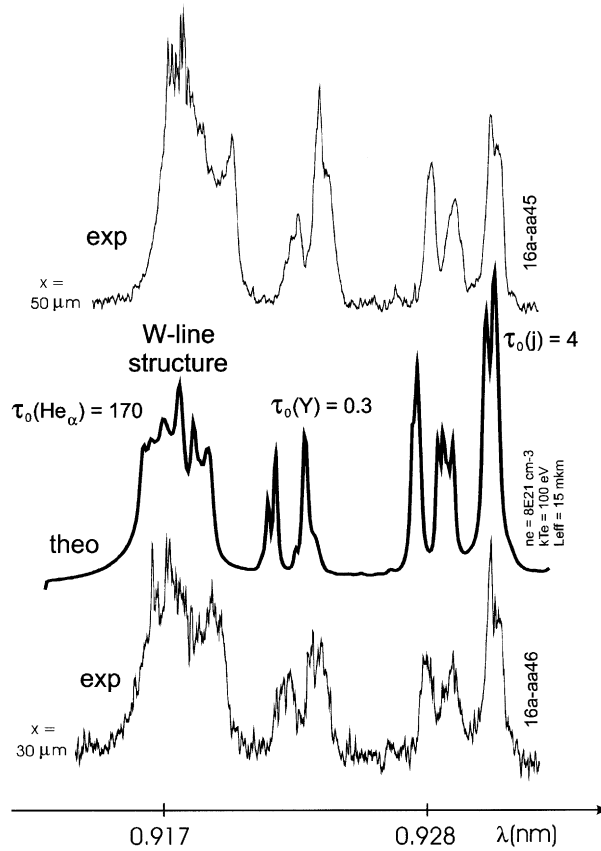


Fig. 10. MARIA-spectrum fitting of the He_α-line of ns-laser experiments assuming the same simulation parameters as obtained in Fig. 6. Good agreement is found cross checking the He_β-simulation results.

He_β-line we find that the line centre optical depth, τ_0 , differs by about a factor of 15:

$$\tau_0 = \frac{1}{4} \lambda_{ji}^2 \frac{g_j}{g_i} A_{ji} n_i \left\{ 1 - \frac{g_i n_j}{g_j n_i} \right\} \varphi_{ij}(\omega = \omega_{ji}) L_{eff} \propto A_{ji} \varphi_{ij}(\omega = \omega_{ji}). \tag{8}$$

Therefore, the He_α-line is more suitable for the determination of the plasma velocity. The parameters determined from the fitting procedure are therefore in agreement, deviations may certainly be caused by the fact that the spectra of Figs. 11a and b have been obtained by different laser shots. The parameters determined from the fittings (Figs. 11a and b) indicate a strongly coupled plasma with a coupling parameter $\Gamma \approx 3-10$.

2.4. Field ionised plasmas: investigation of transitions in hollow ions

Field ionised plasma have been obtained by focussing a CPA Ti-Sapphire laser beam (linear p-polarised) is onto a laminar pulsed nitrogen gas jet with sharp gradients ($L \approx 200 \mu\text{m}$)

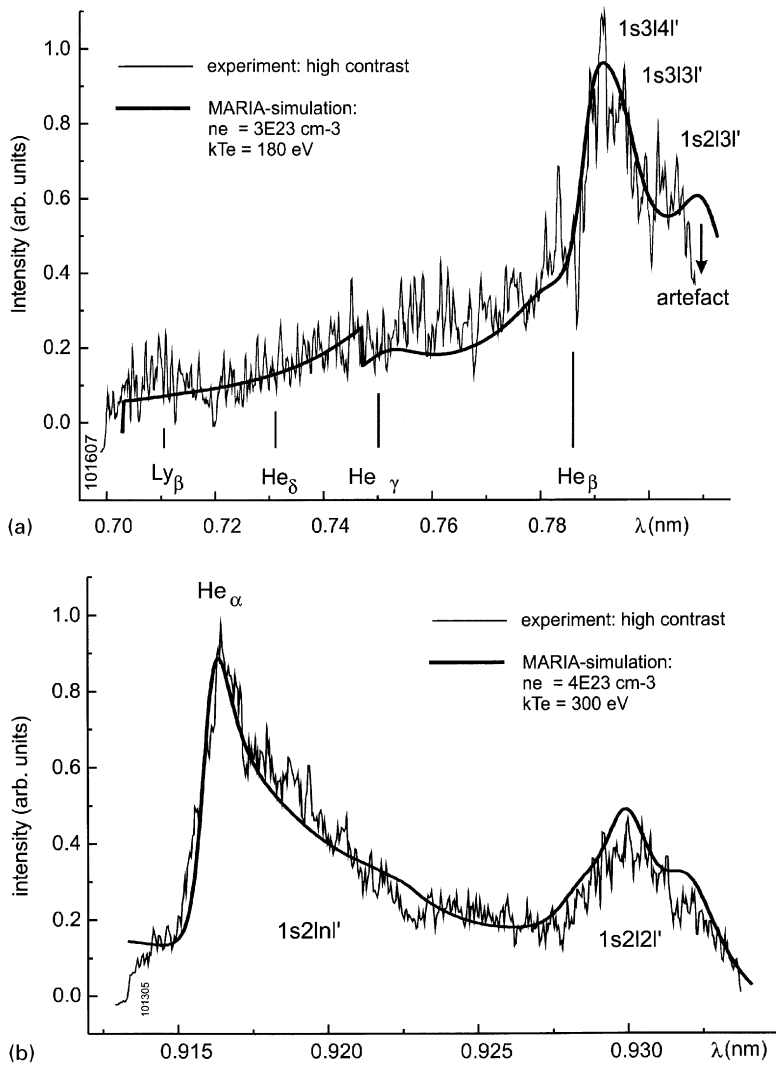


Fig. 11. (a) MARIA calculation of the He β -line up to the series limit for high contrast laser pulses. A reasonable agreement is obtained for $n_e = 3 \times 10^{23} \text{ cm}^{-3}$, $kT_e = 180 \text{ eV}$. Due to high density, the He-like Rydberg series $1snp \ ^1P_1-1s^2$ disappears and the continuum edge is shifted (note that the emission at the long wavelengths interval at about 0.82 nm ends and the intensity drops as an artefact). (b) MARIA calculation of the interval near the He α -line for high contrast laser pulses. The parameters are only slightly different from those obtained from the He β -line due to different laser shots: $n_e = 4 \times 10^{23} \text{ cm}^{-3}$, $kT_e = 300 \text{ eV}$.

and a 20 mm long flat top profile. The density of atoms was $1.5 \times 10^{19} \text{ cm}^{-3}$ for a maximum backing pressure of 20 bar. The energy per pulse was $E = 0.8 \text{ J}$, the wavelength $\lambda = 790 \text{ nm}$ and the contrast is about 10^{-5} at 1 ps. The laser beam with 80 mm diameter is focused with an $f/2.35$ off-axis parabolic mirror 3 mm below the nozzle. The $1/e^2$ focal spot radius is 8 μm . The corresponding Rayleigh length and vacuum intensity are 7 μm and 10^{19} W/cm^2 , respectively. This intensity is able to produce fully stripped nitrogen through field ionisation [35].

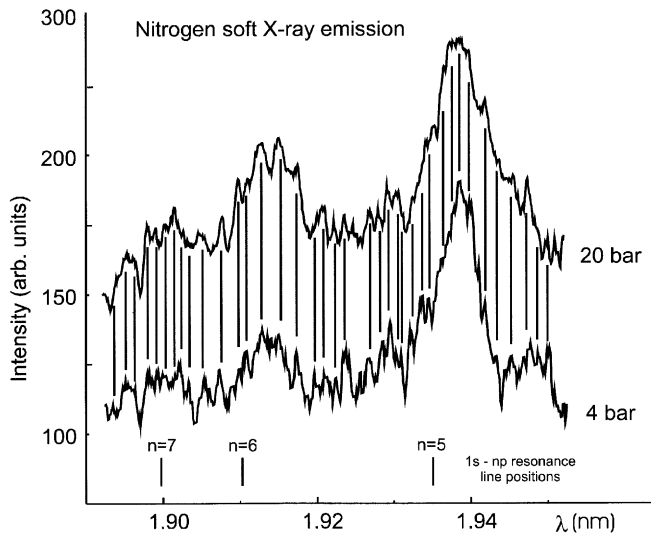


Fig. 12. Experimental spectra of nitrogen recorded at different gas pressures. A clear association of many of the structure inside the broad emission feature near the usual H-like resonance lines 5p, 6p, 7p–1s is seen.

Spatially resolved X-ray spectra of nitrogen have been recorded with spherically bent mica crystals. The crystal, with curvature radius of 150 mm, was placed at a distance of 250 mm from the plasma, with a middle Bragg angle was about 75°. The spectral resolution was $\lambda/\delta\lambda \approx 2000$, and the spatial resolution was $\delta x \approx 30 \mu\text{m}$ in the direction of the laser propagation. X-ray spectra were recorded on Kodak DEF film. The film cassette was protected by 2 layers of polypropylene with thickness 0.8 μm covered by 0.2 μm of Al.

Fig. 12 shows two experimental X-ray spectra of nitrogen in the spectral range from 1.88 to 1.96 nm recorded at different gas pressures. Very broad emission structures around the H-like resonance lines are visible, e.g. at $\lambda \approx 19.12 \times 10^{-10} \text{ m}$, $\lambda \approx 19.36 \times 10^{-10} \text{ m}$. Stark profile calculations show, that for the maximum possible electron density of $n_e \approx 2 \times 10^{20} \text{ cm}^{-3}$ the experimental line widths are much larger than calculated from the Stark broadening. If, however, we compare the experimental spectra in a more detailed manner (see vertical bars) a clear correlation of the numerous structures is discovered. We suggest that these structures to originate from transitions in hollow ions, that is, ions with 2 vacancies in the K-shell:

$$nln'l' \rightarrow \begin{cases} 1sn'l' + \hbar\omega_I \\ 1snl + \hbar\omega_{II} \end{cases} \tag{9}$$

We have used a multi-configuration Hartree–Fock method including relativistic corrections up to the second order, so called HFR-method [30], to calculate wavelengths, transition probabilities and autoionizing rates for these states. For the calculation of atomic data intermediate coupling and configuration interaction have been included. No wavelengths shifts of single transitions or single groups of lines have been done. Pure ab initio calculations (i.e. no scaling parameters are used) are carried out. The following complexes are included (radiative transitions from these states

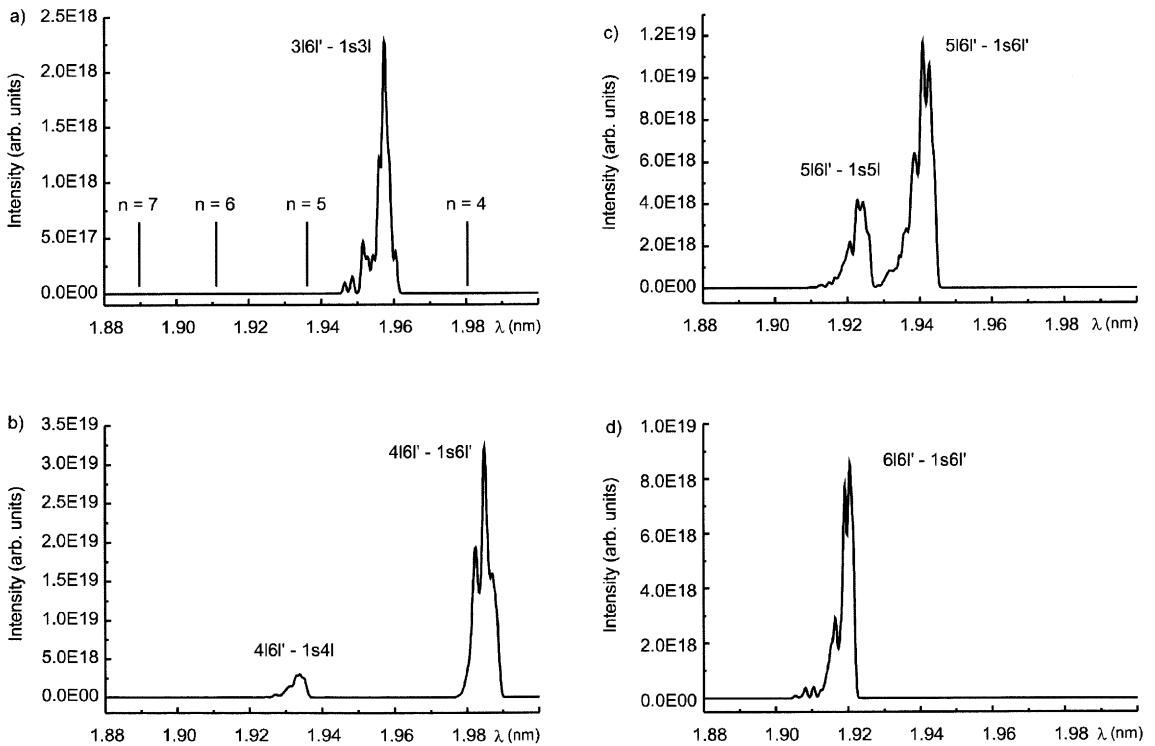


Fig. 13. Spectral distribution of the dielectronic satellite emission originating from the configurations 3l6l', 4l6l', 5l6l' and 6l6l' in hollow nitrogen ions.

are located inside the experimentally observed wavelength interval): 3l5l', 4l5l', 5l5l', 3l6l', 4l6l', 5l6l', 6l6l', 3l7l', 4l7l', 5l7l', 6l7l', 7l7l', 3l8l', 4l8l', 5l8l', 6l8l', 7l8l' and 8l8l'. It can be shown that the total spectral distribution can be reasonably described by

$$I(\omega) \approx \frac{n^0}{g_0} \sum_k \sum_{ij, i \neq j} g_j^k A_{ji}^k \exp(- (E^0 - E^k)/kT_e), \tag{10}$$

where k designates each complex (e.g. $k = 3l6l'$), the transition takes place from the upper level j to the lower level i , E^k are the ionisation energies of the various complexes compared to the nucleus. Fig. 13 shows an example of the spectral distribution originating from the transitions of the complexes 3l6l', 4l6l', 5l6l' and 6l6l'. Very broad emission features as well as emission structure inside the broad features are visible.

Fig. 14 shows the attempt to calculate the spectrum based on satellite transitions in hollow ions (the factor n^0/g_0 is the same for all transitions and therefore omitted in the figures). The agreement is reasonable and resembles many features of the experiment for $kT_e \approx 30$ eV. In particular, the very broad emission features near the positions of the usual H-like resonance lines and the numerous maxima are reflected. The proposed satellite transitions in hollow ions can therefore explain the numerous emission lines in different experiments: differing screening of the nuclear

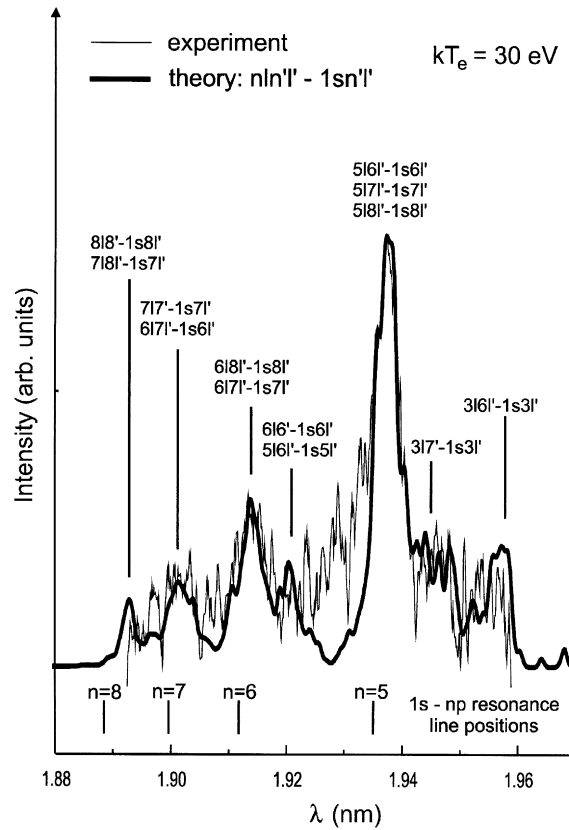


Fig. 14. MARIA-code calculation of nitrogen spectra based on satellites emission in hollow ions. Reasonable agreement is found for $kT_e \approx 30$ eV.

charge due to spectator electrons with different angular momentum coupling and the decay through two radiative channels results in a very broad emission features made up of numerous emission structures as observed in the experiment (see vertical bars in Fig. 12). This can be seen, e.g., in the calculations shown in Fig. 13 where the spectral distribution of the complexes 3l6l', 4l6l' and 6l6l' are presented. The overlap of all the different types of complexes listed above results in a much richer emission feature (the radiative transitions of some complexes are indicated in Fig. 14).

It is worth noting that temperature determined by the spectrum fitting procedure is also in agreement with solutions of the Boltzmann equation [36] which predicted a group of electrons with effective Temperature of $kT_e \approx 40$ eV after some ps. It should be noted that the selection of the emission from the nitrogen “naturally” selects the emission from the recombination regime. The temperature variations according Eq. (10) may therefore be used as a diagnostic of the long-lasting recombination regime based on transitions in hollow ions.

It is interesting that the spectra in Figs. 12 and 13 are reasonably described with transitions from hollow ions only. The question therefore arises what excitation mechanisms result in a high population of the $nln'l'$ -states and leading to strong emission compared to the H-like resonance lines. Charge exchange is proposed [7,37] for the excitation of the $nln'l'$ -states when field ionised

ions penetrate into the residual nitrogen gas, which consists of neutral atoms and singly/doubly ionised ions.

3. Spectroscopic investigations of heavy ion beam heated solid neon

High-energy density matter and the production of dense cold plasmas can be achieved not only with short-pulse high-contrast lasers, but also with heavy ion beams interacting with matter. The advantage of heavy ion beam experiments being the possibility of definite selection of the projectile energy and projectile species. Therefore, the emission of the target and the projectile ions can be adjusted to be suitable for spectroscopic analysis. The disadvantage at present is the insufficient beam intensity to create dense plasmas at the substantial temperatures achievable with lasers. Here we report on the spectroscopic possibilities [17] on the first experiments carried out with the heavy ion accelerator at the GSI in Darmstadt [38,39] using argon ions to interact with solid neon.

A heavy ion beam of Ar_{40}^{18+} with an energy of $E_{\text{beam}} = 300 \text{ MeV/u}$ interacts with a solid neon target. The number of projectile particles is about $N_{\text{beam}} = 1.5 \times 10^{10}$ distributed over a time interval with FWHM of about $\tau = 300 \text{ ns}$. The beam diameter when hitting the target is $d = 1 \text{ mm}$. This provides a “beam density” in the interaction region of

$$n_{\text{beam}} \approx \frac{4}{\pi d^2 \tau c} N_{\text{beam}} \sqrt{1 - \left(\frac{1}{1 + 1.074 \times 10^{-9} E_{\text{beam}}/A_{\text{beam}}} \right)^{2-1}} = 3 \times 10^{20} \text{ cm}^{-3}, \quad (11)$$

where E_{beam} is in eV and A_{beam} is the number of nuclei. This defines a spectroscopic relevant beam fraction [25,40] g_{beam} of

$$g_{\text{beam}} = \frac{n_{\text{beam}}}{n_e}, \quad (12)$$

where n_e is the electron density. Given the value from Eq. (11) the beam fraction in the interaction region could therefore be high enough to influence the ionisation dynamics and the excited states population.

Spectroscopic investigations have been performed in the visible range between 400–700 nm. A 1 m normal incidence VUV spectrometer (VM-521-SG, ACTON RESEARCH CORP.) equipped with a grating of 150 lines/mm was employed which providing an effective resolution of about $\lambda/\delta\lambda \approx 140$, more details are described elsewhere [39]. The spectral interval selects mainly the transitions

$$1s^2 2s^2 2p^5 3\text{LSJ} \rightarrow 1s^2 2s^2 2p^5 3\text{L}'\text{S}'\text{J}' + \hbar\omega.$$

Since the typical temperatures reached are on the order of 0.1 eV after the beam deposition these transitions have several advantages for plasma diagnostics: (1) The splitting inside the 3L SJ levels is large enough to cause a large deviation from the statistical population; and, (2) The absorbing level density for the visible transitions is small because these are themselves excited states. We assume that the spectral distribution can reasonably be described by

$$I(\omega) \approx \frac{n_{\text{gr}}}{g_{\text{gr}}} \sum_{ij, i \neq j} \hbar\omega_{ji} g_j A_{ji} \exp\left(-\frac{\Delta E_j}{kT_e}\right) \Phi_{ji}(\omega_{ji}, \omega). \quad (13)$$

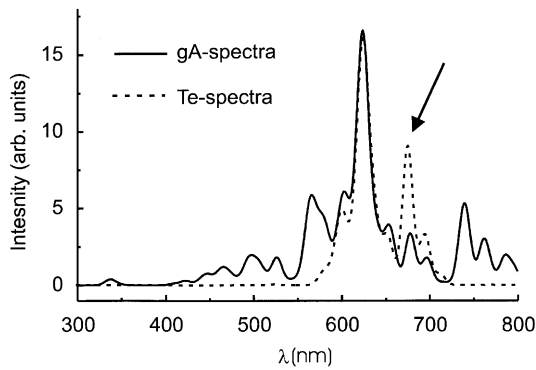


Fig. 15. Temperature dependence of optical neon spectra based on the population variation inside the $1s^2 2s^2 2p^5 3l$ and $1s^2 2s^1 2p^6 3l$ levels using a Boltzmann-factor. For demonstration of the importance of the Boltzmann-factor even in the fine-structure, a spectrum is calculated assuming a statistical population between the various excited nl -levels. The arrow indicates the proposed temperature diagnostic.

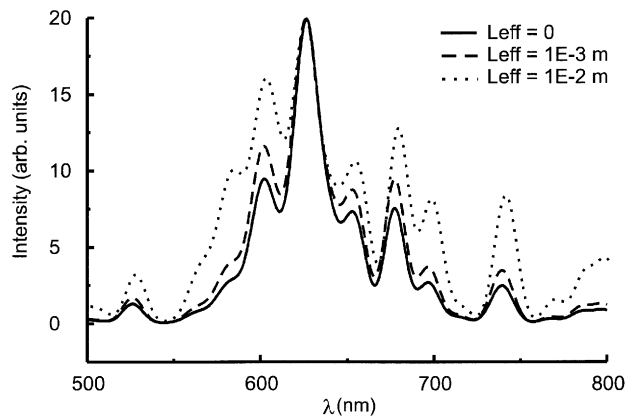


Fig. 16. MARIA-code calculation of the effects of optical depth on the neon spectra in the wavelength interval from 500–800 nm. $kT_e = 1$ eV, ground state density $n(1s^2 2s^2 2p^6 1S_0) = 10^{22} \text{ cm}^{-3}$, $\lambda/\Delta\lambda = 40$.

Here n_{gr}/g_{gr} is the density/statistical weight of the ground state, ω_{ji} is the transition frequency, g_j is the statistical weight of the upper level j , A_{ji} is the radiative decay, ΔE_j is the ionisation energy of the upper level j , T_e is the electron temperature and Φ is the line profile.

Fig. 15 shows the calculations comparing spectra obtained under the assumption of the statistical population of the upper levels (curve “ gA -spectrum”) and the spectrum obtained according Eq. (13) for $kT_e = 0.1$ eV. It can clearly be seen that a large temperature dependence results from the non-statistical population of the upper level configurations $3l$ (note that the gA -spectra do not match with the experiment. Fig. 16 shows the MARIA-code calculations for the optically thick case. For $kT_e = 1$ eV, ground state density $n(1s^2 2s^2 2p^6 1s_0) = 10^{22} \text{ cm}^{-3}$ (note that the absorbing ground states for the considered transitions are the excited states $1s^2 2s^2 2p^5 3l$ and $1s^2 2s^1 2p^6 3l$), opacity effects become visible only for plasma sizes larger than about 1 mm.

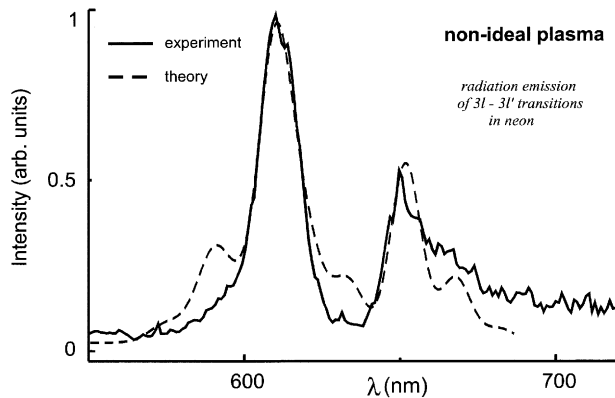


Fig. 17. MARIA-code spectrum fitting assuming no scaling parameters in the atomic data calculations. Quite good agreement is seen for the strong emission structures near 610 and 650 nm for $kT_e \approx 0.18$ eV, $\lambda/\Delta\lambda = 40$.

Fig. 17 shows the experimental time-integrated spectrum. Time resolved measurements have shown that the emission takes place mainly during the interaction of the heavy ion beam with the solid neon. Two pronounced features at $\lambda \approx 610$ and $\lambda \approx 650$ nm are visible. For the calculations, atomic data (wavelengths, transition probabilities, energy levels) have been obtained from the Hartree–Fock code [30] including intermediate coupling and configuration interaction and all states $1s^2 2s^2 2p^6$, $1s^2 2s^2 2p^5 nl$ and $1s^2 2s^1 2p^6 nl$ with $n = 3-6$ and $l = 0-5$ have been included simultaneously. Performing pure ab initio calculations (i.e. no Coulomb scaling parameters are used) the separation of the two maxima match well for $kT_e \approx 0.1$ eV. Smaller “bumps” on the red and blue side of the dominating maxima at $\lambda \approx 610$ nm are also reflected in the calculation, however, in the data these transitions are not so pronounced. The clarification of these discrepancies may provide extended diagnostic possibilities. We note that the temperature estimates based on spectroscopic analysis are also in reasonable agreement with hydrodynamic calculations [39,41] performed with a modified MEDUSA-code version [42].

Finally, we note that these kind of plasmas and their spectroscopic investigations are also of interest for the investigation of non-ideal effects. Taking $kT_e = 0.1$ eV and a density between $n_e = 10^{19}-10^{23}$ cm^{-3} we obtain for the number of particles in the Debye sphere

$$N_D = \frac{1.72 \times 10^9 (kT_e)^{3/2}}{\sqrt{n_e}} \approx 10^{-2} - 10^{-4}. \quad (14)$$

4. Conclusion

New types of X-ray spectra characterised by the disappearance of resonance lines and the dominance of dielectronic satellites have been analysed by means of high-resolution X-ray spectroscopy (spectral resolution $\lambda/\delta\lambda \approx 5000$, spatial resolution $\delta x \approx 10$ μm). Space resolved spectra from ns-laser produced plasmas have been used as a test-bed for the development of theoretical spectra simulations. The He_α and He_β resonance and satellite structure have been successfully

employed for diagnostic purposes. The first investigations of satellite spectra emitted from hollow ions are performed and a temperature diagnostic for the long lasting recombining phase was developed. Their application to high-intensity (10^{19} W/cm²) short (60 fs) laser pulses focused into gas target demonstrate the usefulness of the proposed hollow ion spectroscopy.

For intense high-contrast laser pulses interacting with solid targets very broad emission structures are observed and electron densities up to $n_e \approx 3 \times 10^{23}$ cm⁻³ have been determined. Successful cross cheques involving the spectral window from the He β -line to the Lyman continuum and the He α -emission structure were performed. The electron temperature could be determined with the help of dielectronic satellite spectra and the expansion velocity was determined from the He α line shape analysis in differentially moving optically thick plasmas.

In first heavy ion beams experiments dense plasmas produced with interacting with frozen neon have been spectroscopically investigated. A temperature diagnostic for extremely optically thick dense and cold plasmas was developed and applied to experimental spectra. Successful cross cheques with MHD-calculations are demonstrated.

References

- [1] Boiko VA, Vinogradov AV, Pikuz SA, Skobelev IYu, Faenov AYa. Sov J Laser Research 1985;6:82.
- [2] Griem HR. Principles of plasma spectroscopy. Cambridge: Cambridge University Press, 1997.
- [3] Rosmej FB, Faenov AYa. Phys Scripta 1997;T73:106.
- [4] Rosmej FB, Faenov AYa, Pikuz TA, et al. JETP Lett 1997;65:708.
- [5] Rosmej FB, Faenov AYa, Pikuz TA, et al. JQSRT 1997;58:859.
- [6] Rosmej FB, Faenov AYa, Pikuz TA, et al. J Phys B Lett 1998;31:L921.
- [7] Rosmej FB, Faenov AYa, Pikuz TA, et al. Phys Scripta 1999; T80, in press.
- [8] Faenov AYa, Skobelev IYu, Rosmej FB. Phys Scripta 1999; T80, in press.
- [9] Faenov AYa, Pikuz SA, Erko AI, et al. Phys Scripta 1994;50:333.
- [10] Skobelev IYu, Faenov AYa, Bryunetkin BA, Dyakin VM. JETP 1995;81:692.
- [11] Hölzer G, Förster E, Wolf J, Wehrhan O, Heinisch J, Vollbrecht M, Pikuz TA, Faenov AYa, Pikuz SA, Romanova VM, Shelkovenko TA. Phys Scripta 1998;57:301.
- [12] Aglitskiy Y, Lehecka T, Deniz A, et al. Phys Plasmas 1996;3:3438.
- [13] Faenov AYa, Abdallah J \Jr, Clark REH, et al. Proceedings of SPIE-97. 1997;3157:10.
- [14] Faenov AYa, Magunov AI, Pikuz TA, et al. Phys Scripta 1999; T80, in press.
- [15] Urnov AM, Dubau J, Faenov AYa, et al. JETP Lett 1998;67:489.
- [16] Rosmej FB, Reiter D, Lisitsa VS, et al. Plasma Physics and Controlled Fusion 1999;41:191.
- [17] Funk UN, Bock R, Dornik M, et al. International Conference on the Physics of High Energy Density in Matter. Austria: Hirschegg, 1999.
- [18] Pikuz SA, Maksimchuk A, Umstadter D, et al. JEPT Lett 1997;66:481.
- [19] Maksimchuk A, Nantel M, Ma G, et al. JQSRT 2000;65:367.
- [20] de Michelis C, Matioli M. Nuclear Fusion 1981;21:677.
- [21] Bollanti S, Di Lazzaro P, Flora F, et al. Phys Scripta 1995;51:326.
- [22] Stepanov AE, Starostin AN, Roehrich VC, et al. JQSRT 58;937.
- [23] Rosmej FB. Phys Rev E 1998;58:R32.
- [24] Rosmej FB, Faenov AYa, Pikuz TA, et al. J Phys B 1998;31:L921.
- [25] Rosmej FB. J Phys B 1997;30:L819.
- [26] Rosmej FB, Rosmej ON. J Phys B Lett 1996;29:L359.
- [27] Rosmej FB. Spectroscopic methods for the analysis of plasmas in non-equilibrium, Habilitationsschrift (in german), Ruhr-Universität Bochum, 1998.

- [28] Rosmej FB. Interpretation of X-ray emission spectra from non-equilibrium dense optically thick plasmas: MARIA-code development and atomic data calculations. Report, Institut für Kernphysik, Technische Universität Darmstadt, 1999, in preparation.
- [29] Rosmej FB, Lisitsa VS. *Phys Lett* 1998;A244:401.
- [30] Cowan RD. *Theory of atomic structure and spectra*, Berkeley; University Press, 1981.
- [31] Rosmej FB, Bryunetkin BA, Faenov AYa, et al. *J Phys B* 1996;29:L299.
- [32] Kienle S, Rosmej FB, Schmidt H. *J Phys B* 28;3675.
- [33] Rosmej FB, Abdallah J Jr. *Phys Lett A* 1998;245:548.
- [34] Hummer DG, Mihalas D. *Astr J* 1988;331:794.
- [35] Ammosov MV, Delone NB, Krainov VP. *Sov Phys JETP* 1986;64:1191.
- [36] Andreev NE, Chegotov MV, Veismann ME, et al. *JETP Lett* 1998;68:566.
- [37] Rosmej FB, Faenov AYa, Pikuz TA, et al. *J Phys B* 1998;32:107.
- [38] Funk UN, Bock R, Dornik M, et al. *Nucl. Instr. and Meth. A* 1998;415:68.
- [39] Funk UN. Development and first application of cryogenic production of hydrogen targets designed for experiments with heavy ion beams, Ph.D Thesis (in german), Erlangen, Germany, 1998.
- [40] Rosmej FB. *JQSRT* 1994;51:319.
- [41] Tahir NA, Hoffmann DHH, Maruhn JA, Lutz K-J, Boch R. *Phys Plasmas* 1998;5:4426.
- [42] Tahir NA, Long KA, Laing EW. *J Appl Phys* 1986;60:898.